Materials Today Communications 20 (2019) 100540

Contents lists available at ScienceDirect

Materials Today Communications

journal homepage: www.elsevier.com/locate/mtcomm

Effect of crystalline state on conductive filaments forming process in resistive switching memory devices

Tao Guo[a,1], Hosameldeen Elshekh[b,1], Zhou Yu[c,*], Bo Yu[a], Dan Wang[b], Mayameen S. Kadhim[b], Yuanzheng Chen[b], Wentao Hou[d], Bai Sun[b,*]

[a] State Key Laboratory of Applied Optics, Changchun Institute of Optics and Fine Mechanics, Chinese Academy of Sciences, Changchun 130033, China
[b] School of Physical Science and Technology, Southwest Jiaotong University, Chengdu, Sichuan 610031, China
[c] Ministry of Education of China, and Superconductivity and New Energy R&D Center, Southwest Jiaotong University, Chengdu, Sichuan 610031, China
[d] College of Materials Science and Technology, Nanjing University of Aeronautics and Astronautics (NUAA), Yudao Street 29, 210016 Nanjing, China

ARTICLE INFO

Keywords:
Cu(In, Ga)Se_2
Crystalline state
Conductive filaments
Memory device

ABSTRACT

It is well known that the resistive switching memory is considered as a promising high-performance storage technology to satisfy the demand of information explosion. In this work, the resistive switching memory device with Ag/Cu(In, Ga)Se_2/Mo structure was firstly fabricated, and further the influence of Cu(In, Ga)Se_2 (CIGS) crystalline state on resistive switching performance was investigated. The results show that the HRS/LRS ratio increased from 1.7 to 8.2 as the CIGS layer transferring from amorphous to crystalline, thus the model of crystal state affecting the conductive filament forming process was demonstrated. This work provides an operable method to control the resistive switching performance by tuning the crystal state.

1. Introduction

Explosive development of information technology, such as cloud computing, artificial intelligence and smart phone, starves for higher-performance storage devices with bigger capacity and faster operation speed. However, the flash memory and ferroelectric random access memory (FeRAM) deemed as conventional storage technologies are close to their performance limitation [1,2]. Nowadays, resistive random access memory (RRAM) is regarded as a promising candidate for next generation storage devices, owing to its high-density storage capacity, quick read-write speed and low power consumption [3]. The resistive switching (RS) memory devices are characterized by top-electrode/RS layer/bottom-electrode sandwich structure [4]. The working mechanism of RRAM is resistance value switching between low resistance state (*LRS*) and high resistance state (*HRS*) corresponding to logic '0' and logic '1' [5]. Understanding the RS mechanism is crucial for designing and fabricating practical electronic devices, several methods have been carried out, and great efforts have been made to illustrate the switching mechanism [6–11].

So far, the conducting filament (CF) theory has been extensively used and investigated to demonstrate the RS mechanism. The electrochemical metallization mechanism (ECM) is one of the main CF switching mechanisms for RS devices [12,13]. For ECM device, the active top electrode (Ag [14] or Cu [15]) is required to be oxidized at the interface to form metal cations during the SET process, the generated metal cations then migrate through RS layer towards the bottom electrode under the electronic field force. finally the metal cations will be reduced back to metal atom at the inert bottom electrode (Pt [16]), and the attained atoms will be accumulated to form CF. According to the CF formation procedure in ECM devices, the top electrode is the source of atoms for constructing the CF, so the reactive properties of top electrodes can obviously affect the RS performance [17]. Ahn, Yoonho et al. lately confirmed that the bottom shape can also effectively tune RS performance in Nb/NiO/Nb structures device [18]. The interfaces between electrodes and RS layer are the locations where the redox processes happen, so the state of the interface, such as moisture [19], barrier height [20] interfacial bonding [21], can be relevant to the resistance switching and has been investigated in numerous reports. Thus, the influence of electrodes and interfaces is relatively comprehensive. During the CF forming process, the RS layer acts as solid-electrolyte that provides transfer passage for ions migrating between top-electrode and bottom-electrode under the action of the electric field in RRAM device, so the RS layer properties are extremely important for the CF forming process [22]. The influence of embedded nanoscale metallic inclusions [23], the thickness [24] and the redox rates [25] have been investigated to improve RS performance and clarify

* Corresponding authors.
E-mail addresses: yuzhou@swjtu.edu.cn (Z. Yu), sunbai2010@163.com (B. Sun).
[1] These authors contributed equally to this work.

https://doi.org/10.1016/j.mtcomm.2019.100540
Received 28 May 2019; Accepted 28 May 2019
Available online 29 May 2019

switching mechanism. Besides, crystalline state is one of the most important properties for layer materials and plays a quite important role in thin film devices. However, there are no reports focusing on the influence of RS layer crystalline state on CF forming process. Chalcopyrite Cu(In,Ga)Se_2 (CIGS) is considered as a superior absorber layer owing to its large absorption coefficient ($> 10^5\,cm^{-1}$) and the suitable band gap [26]. The CIGS solar cell has achieved a conversion efficiency record of 22.6%, and it is considered as the most promising thin film solar cell materials [27]. Recently, our previous work found that the CIGS can be used in RRAM devices, and the results illustrate its potential applications in storage technology domain [28].

In this work, the CIGS film was utilized to construct the device with the Ag/CIGS/Mo structure. RS performances, such as resistance window, operation stability and endurance, haves been analyzed systematically. The results show that the CIGS layer crystalline state can affect the RS memory performance obviously. Finally, the model of crystal state affecting conductive filament forming process has been proposed. The model can be extended to different materials in RRAM device systems and presents significant theoretical and practical value.

2. Experimental section

2.1. Fabrication process of device

The CIGS film was deposited on Mo layer by radio-frequency sputtering a single quaternary target with the size of 5 cm-diameter. The work gas was high-pure Ar, the chamber pressure was maintained at o.6 Pa and sputtering power was maintained at 80 W during the sputtering process. The substrate heating was applied (room temperature, 200℃ and 400℃) to obtain different crystallinity, and the corresponding samples are addressed as CIGS (RT), CIGS (200) and CIGS (400) respectively. The thickness of the CIGS films was adjusted to approximately 300 nm by controlling the deposition time. The Ag point electrodes with the size of 1.0 mm^2 was deposited by direct-current (DC) sputtering as the top electrode. Finally, the devices with sandwich structure were obtained, the schematic diagram is shown in Fig. 1a, and the insert gives the photograph of a sample.

2.2. Characteristic

X-ray diffraction (XRD, PANalytical X'Pert PRO system) was carried out to represent the crystalline quality of CIGS film. Scanning electron microscope (SEM, FESEM JOEL 7001, Japan) was used to represent the surface morphology of the CIGS and the cross section of devices. Energy dispersive X-ray spectroscopy (EDX, Inca spectrometer) is used for evaluating the composition. Resistive switching memory property was tested using electrochemical workstation at ambient temperature.

3. Results and discussions

Fig. 1b exhibits the XRD spectra of the CIGS/Mo. The diffraction peak that locates at 40.4° can be observed in all samples, which is corresponding to (110) the plane of the Mo phase [JCPDS file: 00-052-0868]. The film deposited at room temperature does not show diffraction peak except the peak at 40.4°, indicating the CIGS is amorphous. A diffraction peak located at 26.9° corresponding to the (112) plane of CIGS phase [JCPDS: 00-035-1102] can be found as the substrate temperature increased to 200 ℃, which means the CIGS is crystallographic. And the intense increased obviously as the substrate temperature increased to 400 ℃, indicating the crystalline quality is further improved. Fig. 1c shows the cross-section scanning SEM image of the CIGS (400) morphology, the result exhibits that a 300-nm CIGS layer covered on Mo film with good adhesion. Fig. 1d exhibits the EDX spectrum of the CIGS (400) film, confirming Cu, In, Ga, Se constitute the film without any other elements.

The typical *I-V* characteristics of the device were tested with a 0.1 V/ms sweep rate from 0 → 1.0 V → 0 → -1.0 V→ 0, as shown in Fig. 2. Fig. 2a–c show the *I-V* characteristic curves on semilogarithmic scales, the R_{HRS}/R_{LRS} ratio increased from 1.7 to 8.2 as the deposition temperature increased from room temperature to 400℃, and the CIGS with better crystalline quality provides a higher R_{HRS}/R_{LRS} ratio. The operation stability is significantly important for storage devices, so RS performance under repeatedly write-read processes have been investigated. The device with the biggest R_{HRS}/R_{LRS} ratio was chosen to test stability and reliability. The 200 switching loops test on Ag/CIGS (400)/Mo device is shown in Fig. 2d, the result indicates excellent RS

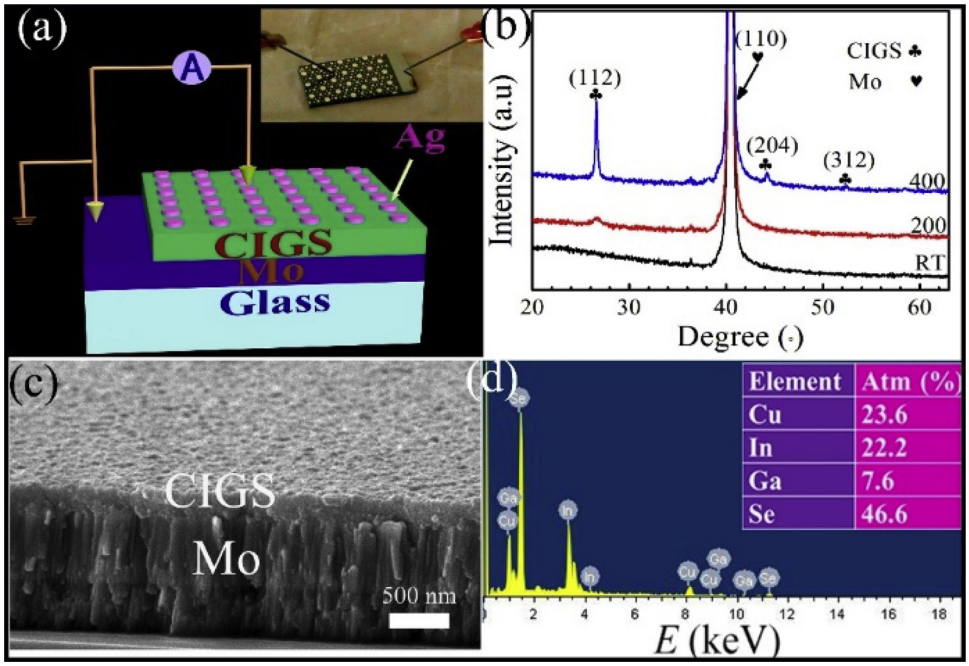

Fig. 1. (a) The structure diagram and the photograph image of the device. (b) The XRD spectra of the CIGS deposited on Mo coated glass under different substrate temperature. (c) The cross-section SEM image of the CIGS/Mo. (d) The EDS spectrum of CIGS film, the atomic ratios are shown in the insert table.

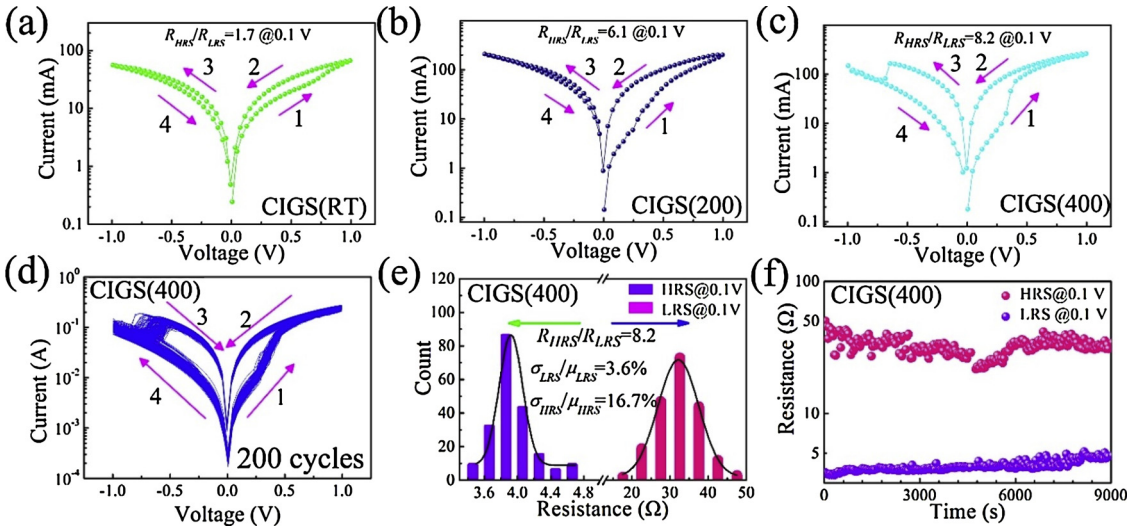

Fig. 2. (a) The single *I-V* sweep curve of the Ag/CIGS(RT)/Mo device on a semilogarithmic scale. (b) The single *I-V* sweep curve of the Ag/CIGS (200)/Mo device on a semilogarithmic scale. (c) The single *I-V* sweep curve of the Ag/CIGS (400)/Mo device on a semilogarithmic scale. (d) 200 *I-V* hysteresis loops of the Ag/CIGS(RT)/Mo device. (e) *HRS* and *LRS* distribution under 0.1 V bias voltage; the σ_{LRS} and σ_{HRS} represent standard deviations, the μ_{LRS} and μ_{HRS} represent mean values, the black line is Gaussian fitting of the bar chart. (f) Retention time of at ON and OFF states under 0.1 V bias voltage.

repeatability. Fig. 2e shows the distribution of *HRS* and *LRS* of Ag/CIGS (400)/Mo device, and the operation voltage was 0.1 V. The *HRS/LRS* ratio is 8.2, the variations (σ/μ) corresponding to *LRS* and *HRS* are 3.6% and 16.7% respectively, indicating stable operation properties [29]. The resistance retention for two states are shown in Fig. 2f, the device exhibits stable resistance states even after 9.0×10^3 s. The above results confirm that the device shows the best resistive switching memory properties when the CIGS layer is deposited under 400℃ with the best crystalline quality.

In this work, the space charge limited conduction (SCLC) model should be responsible for the RS behaviors, which can be described by the Eq. (1) [30]:

$$J \propto \frac{V^{m+1}}{d^{2m+1}} \tag{1}$$

where the J represents current density, the V represents applied voltage, the d represents the thickness of CIGS layer, the m represents fitting index. The *I-V* characteristic obeys Ohmic law ($I \propto V$) as $m = 0$. The *I-V* characteristic obeys Child's square law ($I \propto V^2$) as $m = 1$. when $m = 2$, the current increase sharply under a relatively high bias ($I \propto V^x$, $x > 2$) owing to the conductive filament forming. The Fig. 3 exhibits the *I-V* characteristic cure of the devices on log-log scales. For all devices, the slopes are 1 under low voltage, corresponding to Ohmic conductance behaviors. Then the slopes change to 2.3, 2.5 and 7.6, respectively, as the voltage increased to a relatively high value, indicating the forming of conducting filaments and steep decreasing of resistance. According to the previous work, the Ag electrode can be oxidized easily and forming CF, the process is as follow [22]:

(i) Ag electrode dissolute into ionic:

$$Ag \rightarrow Ag^+ + e^- \tag{2}$$

(ii) Ag^+ drifts across the solid-electrolyte (CIGS) layer under the high electric field [31];

(iii) Ag^+ is reduced and then electro-crystallize on the surface of the inert electrode (Mo):

$$Ag^+ + e^- \rightarrow Ag. \tag{3}$$

(iv) The Ag atoms accumulate gradually to form conducting filament that leads to resistance increase, thus the SET process is completed. And what should be noticed in Ag/CIGS/Mo devices is that the slope of the high voltage region increased from 2.3 to 7.6 as the deposition temperature increased form room temperature to 400℃, the reason is that the conducting filaments show different conductive behavior when the CIGS exhibits different crystalline state, then inducing the difference of RS performance [16,32].

To further demonstrate how the CIGS crystalline state affects the resistive switching performance, the physical model schematic is shown in Fig. 4. The above results have proved that the conducting filament is responsible for RS effects, and the connection and rupture of the conducting filament correspond to the LRS and HRS respectively [33]. The RS layer (CIGS in this work) provides transfer passage for Ag^+ migrating from top-electrode to bottom-electrode under the action of the electric field in Ag/CIGS/Mo RRAM device, so the crystalline state will affect the forming process of the Ag conductive filament significantly. When the RS layer (CIGS) is amorphous, the surface morphology and the cross-section diagrammatic of the device is shown in Fig. 4a. The

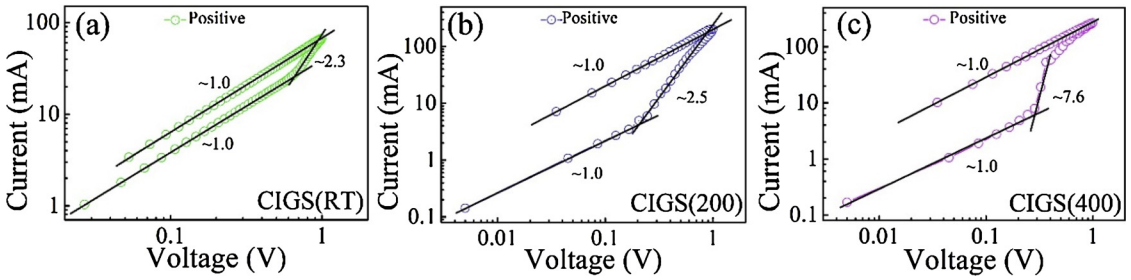

Fig. 3. (a) The *I-V* curve of the Ag/CIGS(RT)/Mo device under *log(I)–log(V)* scale. (b) The *I-V* curve of the Ag/CIGS (200)/Mo device under *log(I)–log(V)* scale. (c) The curve of the Ag/CIGS (400)/Mo device under *log(I)–log(V)* scale.

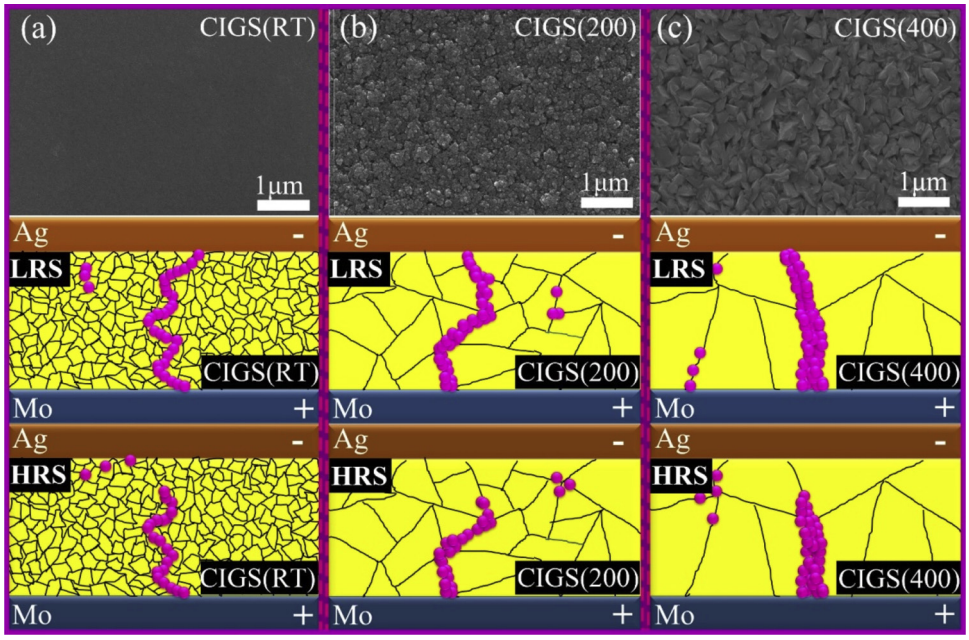

Fig. 4. The physical model schematic of the Ag conducting filament in Ag/CIGS/Mo device.

unordered atoms arrangement causes transport route twisted due to the scattering of Ag^+. So, the CF forming process is restrained and the RS performance is poor. When the RS layer's (CIGS) grain size is increased to approximately 50 nm shown in Fig. 4b, the scattering of Ag^+ during the migration process is lighter, and the device shows better performance but still barely satisfactory. Further improving the crystalline state and the result is shown in Fig. 4c, the grain size is approximately 300 nm, the Ag^+ can diffuse quickly owing less scattering of Ag+, so the CF is easy to form, and the device shows the most excellent RS performance. Besides, the saturation current values (bias voltage at 1.0 V) corresponding to the CIGS (RT), CIGS (200), CIGS (400) are 67 mA, 202 mA, 261 mA, respectively, indicating the thicker conducting filaments formed when the grain sizes are bigger. Therefore, the RS layer crystalline controlling CF forming procedure has been proposed to tune RS performances.

4. Conclusions

In summary, the crystalline state of RS layer (CIGS) on RS performance has been studied. The results show that the CIGS layer with better crystalline state exhibits lighter scattering to Ag^+ diffusion and leads to better RS effects. The model of crystal state affecting conductive filament forming process has been demonstrated. Finally, the *HRS/LRS* ratio of 8.2, the *LRS* variation (σ/μ) of 3.6%, the *HRS* of 16.7%, and excellent endurance in Ag/CIGS(400)/Mo device were obtained. This work can be expanded to different materials in RRAM device systems to regulate and control the RS performance, which presents significant theoretical and practical effects.

Acknowledgement

The authors are grateful for the financial support of the National Magnetic Confinement Fusion Science Program (No. 2013GB110001).

References

[1] C.S. Hwang, Prospective of semiconductor memory devices: from memory system to materials, Adv. Electron. Mater. 1 (2015) 1400056.
[2] M. Gu, X.P. Li, Y.Y. Cao, Optical storage arrays: a perspective for future big data storage, Light Sci. Appl. 3 (2014) e177.
[3] R. Waser, R. Dittmann, G. Staikov, K. Szot, Redox-based resistive switching memories–nanoionic mechanisms, prospects, and challenges, Adv. Mater. 21 (2010) 2632–2663.
[4] D.B. Strukov, G.S. Snider, D.R. Stewart, R.S. Williams, The missing memristor found, Nature 453 (2008) 80–83.
[5] J. Borghetti, G.S. Snider, P.J. Kuekes, J.J. Yang, D.R. Stewart, R.S. Williams, 'Memristive' switches enable 'stateful' logic operations via material implication', Nature 464 (2010) 873–876.
[6] O.L. Muskens, L. Bergamini, Y. Wang, Antenna-assisted picosecond control of nanoscale phase transition in vanadium dioxide, Light Sci. Appl. 5 (2016) e16173.
[7] L. Yao, S. Inkinen, S.V. Dijken, Direct observation of oxygen vacancy-driven structural and resistive phase transitions in $La_{2/3}Sr_{1/3}MnO_3$, Nat. Commun. 8 (2017) 14544.
[8] T. Guo, B. Sun, Z. Yu, H.B. Zhao, M. Lei, Y. Zhao, Overwhelming coexistence of negative differential resistance effect and RRAM, Phys. Chem. Chem. Phys. 20 (2018) 20635–20640.
[9] T. Fujii, M. Kawasaki, A. Sawa, H. Akoh, Y. Kawazoe, Y. Tokura, Hysteretic current–voltage characteristics and resistance switching at an epitaxial oxide Schottky junction $SrRuO_3/SrTi_{0.99}Nb_{0.01}O_3$, Appl. Phys. Lett. 86 (2005) 012107.
[10] G.S. Park, Y.B. Kim, S.Y. Park, X.S. Li, S. Heo, M.J. Lee, M. Chang, J.H. Kwon, M. Kim, U.I. Chung, R. Dittmann, R. Waser, K. Kim, In situ observation of filamentary conducting channels in an asymmetric Ta_2O_{5-x}/TaO_{2-x} bilayer structure, Nat. Commun. 4 (2013) 2382.
[11] U. Celano, L.G.R. Degraeve, A. Fantini, O. Richard, H. Bender, M. Jurczak, W. Vandervorst, Imaging the three-dimensional conductive channel in filamentary-based oxide resistive switching memory, Nano Lett. 15 (2015) 7970–7975.
[12] K.M. Kim, D.S. Jeong, C.S. Hwang, Nanofilamentary resistive switching in binary oxide system; a review on the present status and outlook, Nanotechnology 22 (2011) 254002.
[13] Y. Li, S.B. Long, Q. Liu, H.B. Lv, M. Liu, Resistive switching performance improvement via modulating nanoscale conductive filament, involving the application of two-dimensional layered materials, Small 13 (2017) 1604306.
[14] G. Milano, M. Luebben, Z. Ma, R.D. Borkowski, L. Boarino, C.F. Pirri, R. Waser, C. Ricciardi, I. Valov, Self-limited single nanowire systems combining all-in-one memristive and neuromorphic functionalities, Nat. Commun. 9 (2018) 5151.
[15] S. Gao, C. Song, C. Chen, F. Zeng, F. Pan, Dynamic processes of resistive switching in metallic filament-based organic memory devices, J. Phys. Chem. C 116 (2012) 17955–17959.
[16] Q. Liu, S.B. Long, H.B. Lv, W. Wang, J.B. Niu, Z.L. Huo, J.N. Chen, M. Liu, Controllable growth of nanoscale conductive filaments in solid-electrolyte-based ReRAM by using a metal nanocrystal covered bottom electrode, ACS Nano 4 (10) (2010) 6162–6168.
[17] T. Guo, X.J. Zhang, B. Sun, S.S. Mao, S.H. Zhu, P.P. Zheng, Y.D. Xia, Z. Yu, Effect of electrode materials on nonvolatile resistive switching memory behaviors of metal/In_2S_3/Mo/Glass Devices, J. Electron. Mater. 47 (2018) 5417–5421.
[18] Y. Ahn, H.W. Shin, T.H. Lee, W.H. Kim, J.Y. Son, Effects of Nb nanopin electrode on resistive random-access memory switching characteristics of NiO thin films, Nanoscale 10 (2018) 13443–13448.
[19] S. Tappertzhofen, I. Valov, T. Tsuruoka, T. Hasegawa, R. Waser, M. Aono, Generic relevance of counter charges for cation-based nanoscale resistive switching memories, ACS Nano 7 (2013) 6396–6402.
[20] A. Sawa, T. Fujii, M. Kawasaki, Y. Tokurad, Hysteretic current-voltage characteristics and resistance switching at a rectifying $Ti/Pr_{0.7}Ca_{0.3}MnO_3$ interface, Appl.

Phys. Lett. 85 (2004) 4073–4075.
[21] H. Moon, V. Zade, H.S. Kang, J.W. Han, E. Lee, C.S. Hwang, M.H. Lee, Interfacial chemical bonding-mediated ionic resistive switching, Sci. Rep. 7 (2017) 1264.
[22] I. Valov, R. Waser, J.R. Jameson, M.N. Kozicki, Electrochemical metallization memories-fundamentals, applications, prospects, Nanotechnology 22 (2011) 254003.
[23] Y. Yang, P. Gao, L. Li, X. Pan, S. Tappertzhofen, S. Choi, R. Waser, I. Valov, W.D. Lu, Electrochemical dynamics of nanoscale metallic inclusions in dielectrics, Nat. Commun. 5 (2014) 4232.
[24] Y.C. Yang, P. Gao, S. Gaba, T. Chang, X.Q. Pan, W. Lu, Observation of conducting filament growth in nanoscale resistive memories, Nat. Commun. 3 (2012) 732.
[25] T. Tsuruoka, I. Valov, S. Tappertzhofen, J.V.D. Hurk, T. Hasegawa, R. Waser, M. Aono, Redox reactions at Cu,Ag/Ta_2O_5 interfaces and the effects of Ta_2O_5 film density on the forming process in atomic switch structures, Adv. Funct. Mater. 25 (2015) 6374–6381.
[26] T. Dullweber, G. Hanna, U. Rau, H.W. Schock, A new approach to high-efficiency solar cells by band gap grading in Cu (In, Ga) Se_2 chalcopyrite semiconductors, Sol. Energ. Mat. Sol. C. 67 (2001) 145–150.
[27] P. Jackson, R. Wuerz, D. Hariskos, E. Lotter, W. Witte, M. Powalla, Effects of heavy alkali elements in Cu(In,Ga)Se_2 solar cells with efficiencies up to 22.6%, Phys. Status Solidi RRL 10 (2016) 583–586.
[28] T. Guo, B. Sun, S.S. Mao, S.H. Zhu, Y.D. Xia, H.Y. Wang, Y. Zhao, Z. Yu, A resistance ratio change phenomenon observed in Al doped ZnO (AZO)/Cu ($In_{1-x}Ga_x$) Se_2/Mo resistive switching memory device, Appl. Surf. Sci. 433 (2018) 535–539.
[29] S. Goswami, A.J. Matula, S.P. Rath, S. Hedström, S. Saha, M. Annamalai, D. Sengupta, A. Patra1, S. Ghosh, H. Jani1, S. Sarkar, M.R. Motapothula, C.A. Nijhuis, J. Martin, S. Goswami, V.S. Batista, T. Venkatesan, Robust resistive memory devices using solution-processable metal-coordinated AZO aromatics, Nat. Mater. 16 (2017) 1216.
[30] A. Rose, Space-charge-limited currents in solids, Phys. Rev. 97 (1955) 1538–1544.
[31] P. Han, B. Sun, J. Li, T.J. Li, Q.L. Shi, B.X. Jiao, Q.S. Wu, X.J. Zhang, Ag filament induced nonvolatile resistive switching memory behaviour in hexagonal $MoSe_2$ nanosheets, J. Colloid Interface Sci. 505 (2017) 148–153.
[32] M.S. Kadhim, F. Yang, B. Sun, Y. Wang, T. Guo, Y. Jia, L. Yuan, Y. Yu, Y. Zhao, A resistive switching memory device with a negative differential resistance at room temperature, Appl. Phys. Lett. 113 (2018) 053502.
[33] Z. Lv, Y. Wang, Z. Chen, L. Sun, J. Wang, M. Chen, Z. Xu, Q. Liao, L. Zhou, X. Chen, J. Li, K. Zhou, Y. Zhou, Y.J. Zeng, S.-T. Han, Vellaisamy A.L. Roy, Phototunable biomemory based on light-mediated charge trap, Adv. Sci. 5 (2018) 1800714.